RSC Advances

www.rsc.org/advances

Volume 3 | Number 17 | 7 May 2013 | 5675–6168

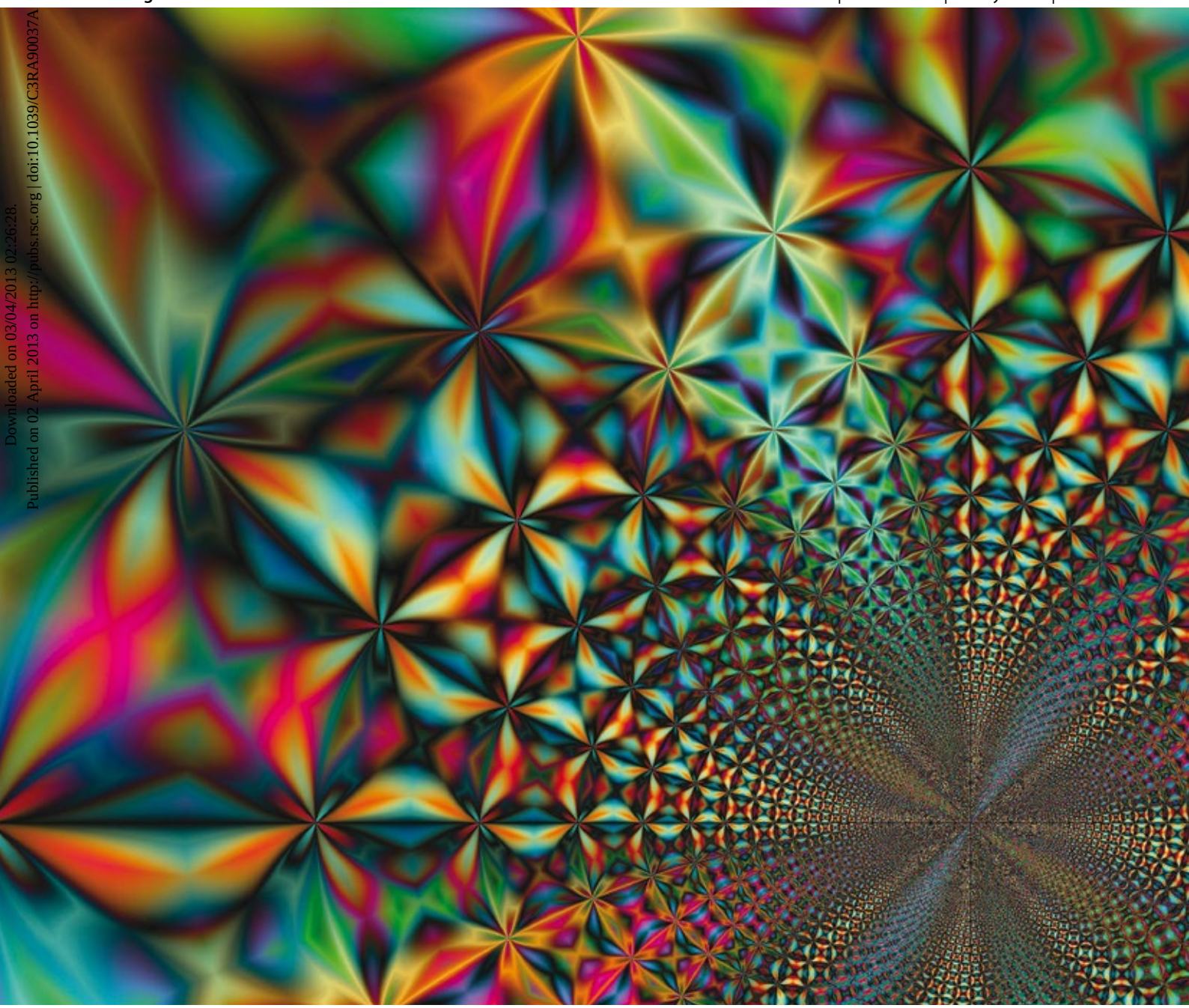

ISSN 2046-2069

RSC Publishing

COMMUNICATIONS

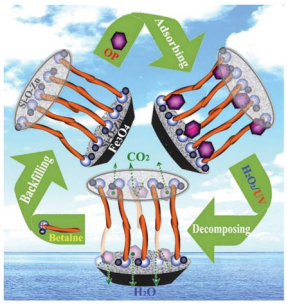

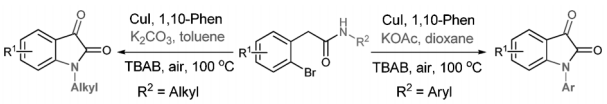

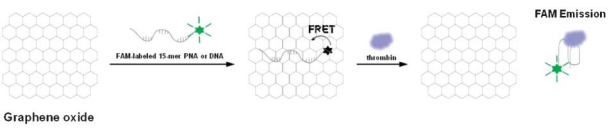

RSC Advances

RSC Publishing

COMMUNICATION

View Article Online
View Journal | View Issue

Selective photodegradation and backfilling for regeneration of the inorganic–organic hybrid composite Fe_3O_4@C_{18}ADB@Zn_2SiO_4 which captures organic pollutants from aqueous solution†

Cite this: *RSC Advances*, 2013, **3**, 5815

Received 27th September 2012,
Accepted 27th February 2013

DOI: 10.1039/c3ra22324h

www.rsc.org/advances

Zheng-Yong Chen, Hong-Wen Gao* and Ya-Yuan He

The Fe_3O_4@C_{18}ADB@Zn_2SiO_4 hybrid composite was synthesized, and it efficiently adsorbed organic pollutants. The resultant dye sludge was degraded by UV–H_2O_2 photocatalysis in the presence of Na_2SO_4, and the sorbent was regenerated by backfilling with C_{18}ADB.

In the past few decades, environmental pollution has become a global problem, with plenty of untreated organic pollutants (OPs) in wastewater posing a serious threat to environmental safety and public health, especially in developing countries.[1] With the development of new technology, environmental functional materials have attracted increasing attention, including OP decomposition materials, such as TiO_2 photocatalytic membranes, adsorption materials *e.g.* chitosan, hydrophobic fraction resins, flocculants *e.g.* chitosan glutamate, and colloidal silica with aluminum fractal polymers.[2] The recently discovered inorganic–organic (IO) hybrid material, as reported in ref. 3, as a host material which shows many advantages in the treatment of pollution, is considered to be an efficient sorbent of dyes, heavy metals and OPs.[3] The sorption ability of this IO material relies on the clever manipulation of the structure of embedded organic compounds, such as rich charges, presence of aliphatic or aryl groups, chelation groups, optical absorption groups and associated steric effects.[4] For example, surfactants containing a hydrophilic and lipophilic structure are often used as soft templates in the control of nanostructured materials.[5] The surfactant–IO hybrid composite exhibits a high adsorption capacity to OPs, *e.g.* ionic dyes and persistent OPs.[3a,6] However, it is difficult for the IO hybrid composite to regenerate. The silicate IO hybrid materials exhibit a high resistance to acids and the capacity for ion exchange, and have hydrophobic character.[3a] One type of amphoteric surfactant, C_{18} alkyl dihydroxyethyl betaine (C_{18}ADB) (Fig. S1A, ESI†) was found to intercalate into zinc silicate to form the Fe_3O_4@C_{18}ADB@Zn_2SiO_4 hybrid composite in the presence of magnetic Fe_3O_4. From the infrared (IR) spectra in Fig. 1B, the Zn–O and Si–O absorption peaks are at 480 and 1020 cm^{-1}. The absorption peaks at 3450, 2870, 2850, 1790 and 1140 cm^{-1} indicate that C_{18}ADB was embedded into the hybrid materials. From the thermal gravimetric analysis (TGA) (Fig. S1A and B, ESI†), a 53% decrease in weight of the hybrid composite indicated that the decomposition of C_{18}ADB occurred between 180 and 500 °C. From the elemental analysis of the hybrid composite, results revealing 42.8% C and 3.9% N indicated that 61% C_{18}ADB was embedded in the hybrid composite, approaching the value calculated from the TGA.

From the small-angle X-ray diffraction (SAXRD) spectra in Fig. 1A, the Fe_3O_4@C_{18}ADB@Zn_2SiO_4 hybrid composite (spectrum 2) showed a layered structure. During the growth of the Zn–O–Si particles in a basic medium, the positively charged amino group of C_{18}ADB (structure shown in Fig. S1A, ESI†) could bind to the negatively charged Zn–O–Si particles *via* electric attraction.[7] Following this, a O–H···O hydrogen bond formed between the hydroxyl and carboxyl groups of C_{18}ADB and Zn_2SiO_4. Because the nano-Fe_3O_4 and Zn–O–Si particles were negatively charged, the positively charged C_{18}ADBs bind to the Fe_3O_4 and Zn–O–Si layers

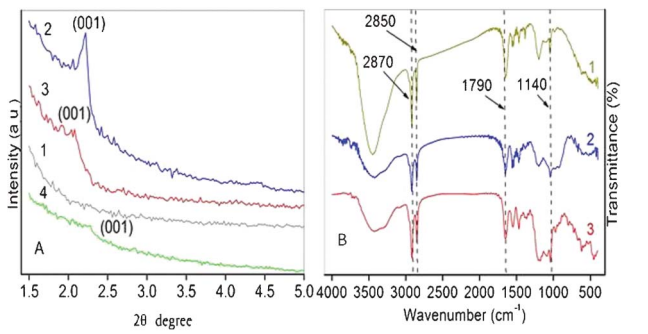

Fig. 1 (A) SAXRD of C_{18}ADB (1), Fe_3O_4@C_{18}ADB@Zn_2SiO_4 (2), Fe_3O&C_{18}ADB(R)@Zn_2SiO_4 (3) and Fe_3O_4&C_{18}ADB@Zn_2SiO_4 residue materials (4) and (B) IR spectra of Zn_2SiO_4 (1), Fe_3O_4@C_{18}ADB@Zn_2SiO_4 (2) and Fe_3O_4&C_{18}ADB(R)@Zn_2SiO_4 (3) materials.

State Key Laboratory of Pollution Control and Resource Reuse, College of Environmental Science and Engineering, Tongji University, Shanghai 200092, China. E-mail: hwgao@tongji.edu.cn; Fax: 86-21-65988598

† Electronic supplementary information (ESI) available: Experimental details, Fig. S1–S6 and Table S1. See DOI: 10.1039/c3ra22324h

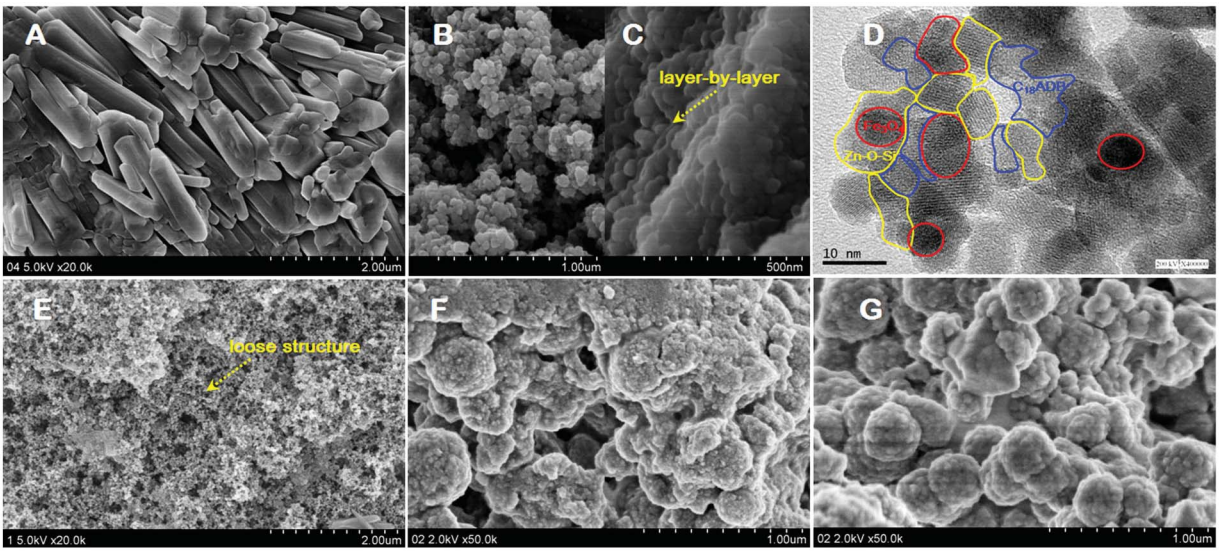

Fig. 2 SEM images of Zn_2SiO_4 (A), the Fe_3O_4@C_{18}ADB@Zn_2SiO_4 hybrid (B: without aging and C: aging for 48 h), the Fe_3O_4@C_{18}ADB(R)@Zn_2SiO_4 (E) and the regenerated sorbent (F: the first and G: the third cycle). (D) Transmission electron microscopy (TEM) of the Fe_3O_4@C_{18}ADB@Zn_2SiO_4 hybrid.

via electric charge attraction. The hydroxyethyl group (–CH_2CH_2OH) of C_{18}ADB may interact with the metal oxides *via* hydrogen bonding, and the carboxyl group (–COOH) of C_{18}ADB could interact with Zn *via* a coordination interaction. In addition, the alkyl chain of C_{18}ADB, with a length of 2.7 nm (Fig. S1A, ESI†), may further interact *via* a hydrophobic stack. Thus, the C_{18}ADB bilayer was fixed between the Zn_2SiO_4 particles with an interval of 4.2 nm (Fig. 1A).

The scanning electron microscopy (SEM) images (Fig. 2A) show that Zn_2SiO_4 is columnar, the columns being 1–3 μm in length and 200–300 nm in width. After C_{18}ADB and Fe_3O_4 were coated and embedded, many particles of approximately 50 nm adhered together to form a reticular structure (Fig. 2B), and aged into the layer-by-layer material (Fig. 2C). Just like an adhesive, C_{18}ADB bridged the Zn–O–Si layers and some of the Fe_3O_4 to alter the morphology of the Fe_3O_4@C_{18}ADB@Zn_2SiO_4 hybrid composite, where the stripes (red and yellow) of the Fe_3O_4 and Zn_2SiO_4 crystal grains and the irregular interlayer (blue) of the C_{18}ADB appeared (Fig. 2D). Another Fe_3O_4 layer was coated by C_{18}ADB *via* hydrogen bonds in the process of synthesizing the materials.

Differing from the other hybrid composite synthesized previously,[3a] the above hybrid composite may capture cationic and anionic dyes simultaneously from aqueous solutions, owing to many embedded amphoteric C_{18}ADB units, which is confirmed from its ζ-potentials changing from +13.6 to −36.8 mV between pH 3 and 10 (Fig. S1C, ESI†). The sulfonic dyes reactive brilliant red X-3B and congo red, and the cationic dyes victoria blue BO and rhodamine B, were tested for adsorbtion by the Fe_3O_4@C_{18}ADB@Zn_2SiO_4 hybrid composite, and the adsorption obeyed the Langmuir isotherm model, $c_e/q_e = 1/K_aq_\infty + c_e/q_\infty$[8] ($c_e$, q_e and q_∞ represent the equilibrium molarity, equilibrium adsorption value and saturation value of the dye and K_a represents the adsorption constant) (Fig. 3A and B). Their q_∞ values were calculated to be 464, 769, 406 and 117 mg g^{-1} respectively, superior to the other sorbents.[8] Their K_a values were calculated to be 7.11 × 10^3, 6.84 × 10^3, 9.20 × 10^3 and 1.76 × 10^4 M^{-1} respectively. In addition to the electric attractions and hydrogen bonding, a hydrophobic interaction will form between the hydrophobic group of the dye and the long alkyl chain of C_{18}ADB. The adsorption equilibrium is reached in 10 min (Fig. S2A, ESI†), which is much faster than that of activated carbon.[9] In addition, the adsorption capacities (q_∞) of the hybrid to the dyes approach that of activated carbon[9] but its surface area of 3.6 m^2

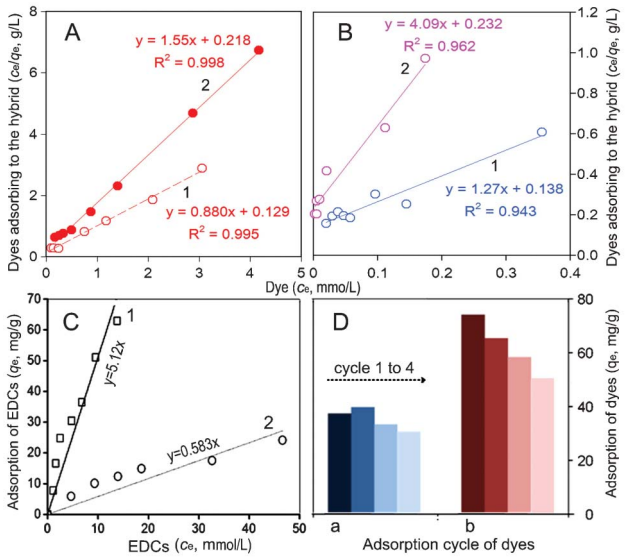

Fig. 3 Adsorption of congo red (A1), reactive brilliant red X-3B (A2), victoria blue BO (B1), rhodamine B (B2), NP (C1) and BPA (C2) to the Fe_3O_4@C_{18}ADB@Zn_2SiO_4 hybrid composite. D: cycles 1–4 of 0.10 mM victoria blue BO (a), and 0.25 mM reactive brilliant red X-3B (b) adsorbed to 0.05% of the Fe_3O_4@C_{18}ADB@Zn_2SiO_4 hybrid composite (cycle 1) and the regenerated sorbent (cycles 2–4).

g^{-1} is much smaller than that of activated carbon. The ζ-potential of the hybrid composite approached 0 after the adsorption of congo red and victoria blue BO. As a result, the charge attraction played a primary role in the adsorption of the ionic dyes,[3a] *i.e.* the embedding of C_{18}ADB into the hybrid composite captured ionic dyes from the aqueous solution.

The pH of the solution affected the adsorption of the dyes. The q_e of congo red remained almost constant between a pH of 3.6 and 8, and decreased by 40% at pH 11. On increasing the pH from 3.6 to 8, the q_e of victoria blue BO decreased by 57% (Fig. S2B, ESI†). The adsorption of the dyes increased with an increase in ionic strength (Fig. S2C, ESI†). The q_e of congo red and victoria blue BO increased by 136% and 68% in 0.3 M NaCl, respectively. Therefore, the hybrid sorbent prepared is favorable for the treatment of the high-salinity dye wastewater.

The endocrine disrupting compounds (EDCs) represented in this study, bisphenol A (BPA) and nonylphenol (NP), often appear in nature.[10] Being different from the above dyes, they were adsorbed onto the Fe_3O_4@C_{18}ADB@Zn_2SiO_4 hybrid composite according to the lipid–water partition law (Fig. 3C). Their partition coefficients (K_{aw}) were calculated to be 2660 and 8790 L kg^{-1}. Only 0.05% of the hybrid composite removed 60% BPA and 80% NP (Fig. S3, ESI†), which is similar to the traditional sorbents *e.g.* activated carbon and polymers.[11] The dyes may dissolve into the C_{18}ADB bilayer stack embedded in the hybrid composite *via* hydrophobic interactions.[12] The adsorption of NP was completed in 10 min (Fig S2D, ESI†) and remained at a constant maximum between a pH of 4.2 and 8.5 (Fig S2E, ESI†).

The regeneration of sorbents including acids/alkalis and organic solvent washing and calcination often leads to the high consumption of energy and resources.[13] The degradation of the resultant dye-Fe_3O_4@C_{18}ADB@Zn_2SiO_4 sludge by UV–H_2O_2 photocatalysis was tested. The dye color almost disappeared under UV light after 50 min in 4 M H_2O_2 (Fig. S4A and B, ESI†). However, the addition of Na_2SO_4 resulted in the largest apparent volume of the sludge (Fig. S4C, ESI†), *i.e.* the layered structure of the hybrid sorbent was destroyed in the absence of Na_2SO_4. Microscopic images confirmed that Na_2SO_4 made the final sludge particles quite loose (Fig. S5, ESI†). The elemental analysis indicated that the C content gradually decreased with increasing photocatalytic time (Table S1, ESI†). This may be attributed to the complete decomposition of the dye and C_{18}ADB. Inorganic salts, sodium chloride and sodium sulphate, were added in order to prevent the destruction of the structure. The results indicated that sodium chloride is almost non-effective. In the presence of 0.25 M Na_2SO_4, lots of closely linked nanosized particles were supported (Fig. 2E). The elemental analysis indicated that the residue contained 26.7% C, *i.e.* 37.6% C_{18}ADB was decomposed during the photocatalytic degradation. Escaping CO_2 and H_2O from decomposition of the dye and C_{18}ADB may puncture the layered zinc silicate (Fig. 2E). It is possible for large amounts of SO_4^{2-} to insert into the layered zinc silicate, replacing the decomposed dye and C_{18}ADB, thus supporting the layered structure, where SO_4^{2-} may bind immediately with Zn by O–Zn complexation. The Fe_3O_4 and residual C_{18}ADB(C_{18}ADB(R))@Zn_2SiO_4 residue may be formed and it was mixed with 0.07 M C_{18}ADB for regeneration. The formed particles remained in the layered structure with an interval of 4.0 nm calculated from spectrum 3 in Fig. 1A, which is close to that of the freshly prepared Fe_3O_4@C_{18}ADB@Zn_2SiO_4 hybrid composite. The C content increased to 36.0% in the regenerated sorbent. In addition, 60% of the regenerated sorbent's weight loss from 180 to 500 °C (Fig. S1A and B, ESI†) indicated that the C_{18}ADB content was close to that of the freshly prepared hybrid composite. Thus, the backfilling of C_{18}ADB occurred, *i.e.* the Fe_3O_4@C_{18}ADB@Zn_2SiO_4 sorbent was successfully regenerated. It may be attributed to SO_4^{2-} being able to generate peroxydisulfate ($S_2O_8^{2-}$) from UV–H_2O_2 photocatalysis,[14] which would reduce the rate of photocatalysis. In this case, the oxidation properties of $S_2O_8^{2-}$ was inferior to that of $HO^{\bullet}$, so that the rate of the decomposition of C_{18}ADB was low. Then, the structure of C_{18}ADB bilayer was preserved with the interval of 4.0 nm (spectrum 4 in Fig. 1A). However, the regenerated particles appeared to be spherical with 200–500 nm size (Fig. 2F), which is a different morphology to that of the freshly prepared hybrid composite (Fig. 2B). It is possible that C_{18}ADB attracted the loose Zn_2SiO_4 nanoparticles (Fig. 2E), which aggregated together and then aged into the I–O–I–O layered sphere.

The first regenerated sorbent was used to adsorb victoria blue BO and reactive brilliant red X-3B. The adsorption values of the dyes were close to those with the freshly prepared hybrid composite (Fig. 3D and Fig. S4E, ESI†). The dye sludge was repeatedly regenerated by the same method as above. The third regenerated sorbent remained spherical (Fig. 2G). The adsorption of the dyes decreased by 10% every cycle (Fig. 3D). This is due to some loss of the C_{18}ADB backfilling during the regeneration of the sorbent.

Being convenient for use in contamination control, magnetic particles are often embedded.[15] Fe_3O_4 was added to complex with Zn_2SiO_4 and C_{18}ADB. The magnetization of the Fe_3O_4@C_{18}ADB@Zn_2SiO_4 hybrid composite was measured as 10 emu g^{-1} (Fig. S6E, ESI†). Thus, the magnetic separation of the hybrid composite is complete in 10 min (Fig. S6A–D, ESI†). The regenerated sorbent remained at a magnetization of 7 emu g^{-1}. Consequently the regeneration process did not seriously decrease the magnetic performance of the sorbent.

In conclusion, this work provided facile regeneration of the IO hybrid material by UV–H_2O_2 photocatalysis in sodium sulphate solution and the backfilling of the functional organic compound. It is very important not only in environmental pollution control but also in the saving of resources and energy.

The authors acknowledge the financial support from The National Key Technology R&D Program of China (Grant No. 2013BAC01B01) and The Foundation of State Key Laboratory of Pollution Control and Resource Reuse (Tongji University), China (PCRRK11003).

Notes and references

1 (*a*) P. Webster, *Science*, 2004, **306**, 1875a; (*b*) M. Yang, J. W. Yu, Z. L. Li, Z. H. Guo, M. Burch and T. F. Lin, *Science*, 2008, **319**, 158a.

2 (*a*) H. Choi, A. C. Sofranko and D. D. Dionysiou, *Adv. Funct. Mater.*, 2006, **16**, 1067; (*b*) C. Gerente, V. K. C. Lee, P. Le Cloirec

and G. McKay, *Crit. Rev. Environ. Sci. Technol.*, 2007, **37**, 41; (*c*) M. L. Quaranta, M. D. Mendes and A. A. MacKay, *Water Res.*, 2012, **46**, 284; (*d*) S. Bratskaya, S. Schwarz and D. Chervonetsky, *Water Res.*, 2004, **38**, 2955; (*e*) B. S. Lartiges, J. Y. Bottero, L. S. Derrendinger, B. Humbert, P. Tekely and H. Suty, *Langmuir*, 1997, **13**, 147.

3 (*a*) Y. P. Wei and H. W. Gao, *J. Mater. Chem.*, 2012, **22**, 5715; (*b*) F. Ciesielczyk, A. Krysztafkiewicz and T. Jesionowski, *J. Mater. Sci.*, 2007, **42**, 3831.

4 (*a*) G. Decher, *Science*, 1997, **277**, 1232; (*b*) D. Y. Zhong, J. H. Franke, S. K. Podiyanachari, T. Blomker, H. M. Zhang, G. Kehr, G. Erker, H. Fuchs and L. F. Chi, *Science*, 2011, **334**, 213; (*c*) M. C. B. Sheng Dai, Y. H. Ju and H. J. Gao, *J. Am. Chem. Soc.*, 2000, **122**, 992; (*d*) M. Kimura, R. Sakai, S. Sato, T. Fukawa, T. Ikehara, R. Maeda and T. Mihara, *Adv. Funct. Mater.*, 2012, **22**, 469; (*e*) A. B. Thompson, S. J. Cope, T. D. Swift and J. M. Notestein, *Langmuir*, 2011, **27**, 11990.

5 Y. Wan and D. Zhao, *Chem. Rev.*, 2007, **107**, 2821.

6 (*a*) A. R. Auxilio, P. C. Andrews, P. C. Junk, L. Spiccia, D. Neumann, W. Raverty, N. Vanderhoek and J. M. Pringle, *J. Mater. Chem.*, 2008, **18**, 2466; (*b*) D. G. Kurth, F. Caruso and C. Schuler, *Chem. Commun.*, 1999, 1579; (*c*) R. Sasai, N. Iyi, T. Fujita, F. L. Arbeloa, V. M. Martinez, K. Takagi and H. Itoh, *Langmuir*, 2004, **20**, 4715.

7 C. J. Meledandri, J. K. Stolarczyk and D. F. Brougham, *ACS Nano*, 2011, **5**, 1747.

8 (*a*) Z. Song, L. F. Chen, J. C. Hu and R. Richards, *Nanotechnology*, 2009, **20**, 275707; (*b*) Y. Liu, Y. P. Guo, W. Gao, Z. Wang, Y. J. Ma and Z. C. Wang, *J. Clean. Prod.*, 2012, **32**, 204.

9 L. Sun, C. G. Tian, L. Wang, J. L. Zou, G. Mu and H. G. Fu, *J. Mater. Chem.*, 2011, **21**, 7232.

10 E. Diamanti-Kandarakis, J. P. Bourguignon, L. C. Giudice, R. Hauser, G. S. Prins, A. M. Soto, R.T. Zoeller and A. C. Gore, *Endocr. Rev.*, 2009, **30**, 293.

11 (*a*) H. Y. Niu, Y. Q. Cai, Y. L. Shi, F. S. Wei, J. M. Liu and G. B. Jiang, *Anal. Bioanal. Chem.*, 2008, **392**, 927; (*b*) T. Asada, K. Oikawa, K. Kawata, S. Ishihara, T. Iyobe and A. Yamada, *J. Health Sci.*, 2004, **50**, 588; (*c*) T. Basile, A. Petrella, M. Petrella, G. Boghetich, V. Petruzzelli, S. Colasuonno and D. Petruzzelli, *Ind. Eng. Chem. Res.*, 2011, **50**, 8389.

12 P. Wang, Q. H. Shi, Y. F. Shi, K. K. Clark, G. D. Stucky and A. A. Keller, *J. Am. Chem. Soc.*, 2009, **131**, 182.

13 (*a*) S. J. Wu, F. T. Li, Y. N. Wu, R. Xu and G. T. Li, *Chem. Commun.*, 2010, **46**, 1694; (*b*) S. H. Tolbert, A. Firouzi, G. D. Stucky and B. F. Chmelka, *Science*, 1997, **278**, 264.

14 D. Salari, A. Niaei, S. Aber and M. H. Rasoulifard, *J. Hazard. Mater.*, 2009, **166**, 61.

15 P. G. Wu, J. H. Zhu and Z. H. Xu, *Adv. Funct. Mater.*, 2004, **14**, 345.

